Chemical Physics Letters 512 (2011) 30–34

Contents lists available at ScienceDirect

Chemical Physics Letters

journal homepage: www.elsevier.com/locate/cplett

Three-body photodissociation dynamics of $I_2^-(CO_2)$

Aaron W. Harrison, Jeong Sik Lim, Paul E. Crider [1], Daniel M. Neumark *

Department of Chemistry, University of California, Berkeley, CA 94720, USA
Chemical Sciences Division, Lawrence Berkeley National Laboratory, Berkeley, CA 94720, USA

ARTICLE INFO

Article history:
Received 27 May 2011
In final form 1 July 2011
Available online 7 July 2011

ABSTRACT

The three-body dissociation of $I_2^-(CO_2)$ following excitation of the I_2^- chromophore to the repulsive $A'^2\Pi_{g,1/2}$ and $B^2\Sigma^+_{g,1/2}$ electronic states at 1.72 and 3.21 eV has been investigated using fast beam photofragment translational spectroscopy. The translational energy distributions for three-body dissociation provide a direct measurement of the CO_2 binding energy, yielding a value of 218 ± 10 meV. These distributions are vibrationally resolved and show that some CO_2 is produced with bend excitation. Dalitz plots show that the dominant three-body decay mechanism is asynchronous–concerted decay, in which the two bond cleavages are distinct but nearly simultaneous events.

1. Introduction

The formation and cleavage of molecular bonds in chemical reactions is one of the most fundamental concepts in all of science. Scattering measurements such as crossed molecular beams experiments probe this process in exquisite detail in bimolecular reactive collisions [1]. Complementary information on unimolecular dynamics is obtained from photodissociation experiments, in which absorption of a single photon with well-defined energy results in the rupturing of one or more chemical bonds, thereby providing invaluable insights into the mechanism by which vibrational or electronic excitation is coupled to molecular dissociation [2,3]. The vast majority of these studies have focused on two-body dissociation; photodissociation into three fragments remains less explored largely owing to the difficulty of obtaining a complete picture of these complex decay pathways [4,5]. However, photofragmentation into three (or more) fragments has been inferred in species such as H_3 [6], $COCl_2$ [4], and glyoxal [7]; three-body dissociation is also seen in collision-induced dissociation [8], dissociative photodetachment [9], and dissociative charge exchange [10]. The mechanism by which these three-body dissociation reactions occur (concerted vs. sequential) is a topic of much interest in reaction dynamics. It is particularly fruitful to study these dynamics is using fast beam dissociation experiments that are capable of making time and position sensitive measurement of all coincident photofragments [6,10–12]. This methodology offers a complete picture of the fragmentation and allows elucidation of both energetic and mechanistic information.

In this Letter, the three-body photodissociation of the ion–molecule complex $I_2^-(CO_2)$ is investigated. Photodissociation of I_2^- following excitation into the repulsive $A'^2\Pi_{g,1/2}$ and $B^2\Sigma^+_{g,1/2}$ electronic states has been studied extensively, not only as an isolated species in the gas phase [13,14], but also in charged clusters with various solvating species [15–19] and in bulk solution [20,21]. As such, the ease of formation and mass selection of $I_2^-(CO_2)_n$ clusters in the gas phase coupled with the energetic accessibility of the three-body dissociation limit makes $I_2^-(CO_2)$ an excellent model system for the study of three-body decay. Prior to dissociation, the I_2^- chromophore is largely unperturbed by the presence of CO_2 [15], but the addition of just one solvent molecule can be sufficient to alter the dissociation dynamics. For example, Lineberger and co-workers [22,23] have shown that in the photodissociation of a very similar system, $IBr^-(CO_2)$, the CO_2 molecule mediates a long-range electron transfer between the separating halogens. This interaction results in a small amount of Br^- + I products upon excitation of the A' state of $IBr^-(CO_2)$, whereas in the bare diatomic the A' state dissociates solely to I^- + Br.

Anion photoelectron spectroscopy of $I_2^-(CO_2)$ [24] reveals a progression in the CO_2 bending mode, indicating that the CO_2 is slightly bent in the anion. As part of that study, electronic structure calculations and Franck–Condon analysis determined that the ground-state geometry is of C_{2v} symmetry in which the CO_2 is bound at the I_2^- waist with an OCO bond angle of approximately 177.5°; the CO_2 lies in a plane that perpendicularly bisects the I–I internuclear axis. Population analysis showed some charge transfer into the π^* LUMO of CO_2, which would favor a bent geometry, but the distortion can also result from electrostatic interactions [25,26]. The strong charge-quadrupole interaction of the electropositive carbon and the negatively charged I_2^- leads to relatively large solvation energies in these clusters. Cluster calorimetry was used to determine these energies over a range of cluster sizes [27] and yielded a binding energy of 234 ± 21 meV for the first

* Corresponding author at: Department of Chemistry, University of California, Berkeley, CA 94720, USA. Fax: +1 510 642 3635.
E-mail address: dneumark@berkeley.edu (D.M. Neumark).
[1] Present address: Institut fur Physikalische Chemie, Karlsruhe Institut furTechnologie (KIT), Karlsruhe 76128, Germany.

0009-2614/$ - see front matter © 2011 Elsevier B.V. All rights reserved.
doi:10.1016/j.cplett.2011.07.001

CO_2. In this method, the anion binding energy is extrapolated by measuring the shift in vertical detachment energy of I_2^- over a range $I_2^-(CO_2)_n$ cluster sizes. Recent electronic calculations on the microsolvation of $I_2^-(CO_2)_n$ clusters [26] are in substantial agreement with the experimental binding energy, finding values of 224 and 232 meV at the MP2 and CCSD(T) level of theory, respectively.

Herein, we report a kinematically complete study of the three-body photodissociation of $I_2^-(CO_2)$ by coincidence imaging of the recoiling photofragments following dissociation of a fast beam of parent ions. Results are presented for dissociation of $I_2^-(CO_2)$ following excitation of the I_2^- chromophore into the $A'^2\Pi_{g,1/2}$ state at 720 nm and the $B^2\Sigma^+_{g,1/2}$ state at 386 nm. The three-body translational energy distributions show resolved structure resulting from vibrational excitation of the CO_2 fragment and directly yield the $I_2^- \cdot\cdot CO_2$ binding energy. Analysis using Dalitz plots probes the detailed three-body decay mechanism. Differences in the CO_2 vibrational distribution and Dalitz plots at the two wavelengths are observed and discussed.

2. Experimental

The current study was performed on our fast beam photofragment translational spectrometer that has been described in detail elsewhere [28,29]. Briefly, $I_2^-(CO_2)$ cluster ions are produced by flowing a mixture of 10% CO_2 seeded in O_2 (25 psig) over iodine crystals (neat O_2 for bare I_2^-) and subsequently expanding this mixture into a vacuum chamber through a pulsed piezoelectric valve operating at 60 Hz. This free jet expansion is intersected downstream by a continuous 1 keV electron beam, and the resulting ions are accelerated to a laboratory frame beam energy of 8 keV. Mass selection is achieved by a Bakker time-of-flight mass spectrometer [30,31] that imparts negligible kinetic energy spread to the ion beam. The ion packet of interest is then intersected with a pulse from a Lambda–Physik XeCl excimer-pumped dye laser system (FL 3002 and Scanmate at 720 and 386 nm, respectively) polarized in the plane of the detector. The recoiling photofragments are detected 2.15 m downstream by a time and position sensitive (TPS) detector, while undissociated parent ions are intercepted by a 5 mm diameter beam block.

The TPS detector comprises three 75 mm diameter microchannel plates in a Z-stack and coupled to a phosphor screen. The image from the phosphor screen is split by a dichroic beam splitter to a photomultiplier tube and CCD camera for relative timing and position information, respectively [32]. Analysis of this data yields the photofragment masses, the center-of mass translational energy release E_T, and the recoil angle with respect to the to the polarization of the laser beam for two-body dissociation. In the case of the three-body dissociation, the center of mass momenta of each fragment are calculated providing additional mechanistic information about the fragmentation through the use of Dalitz plot analysis [33].

3. Results and discussion

3.1. Translational energy distributions

Figure 1 shows the photofragment translational energy dissociation for the two-body dissociation of I_2^- and the three-body dissociation of $I_2^-(CO_2)$ following excitation of the $A'^2\Pi_{g,1/2} - X^2\Sigma^+_{u,1/2}$ transition of I_2^- at 720 nm (1.722 eV). Figure 2 shows the analogous results from excitation of the $B\,^2\Sigma^+_{g,1/2}$ state at 386 nm (3.212 eV). In both cases, the excited I_2^- state is repulsive in the Franck–Condon region [34]; the $A'^2\Pi_{g,1/2}$ state correlates to $I^- + I(^2P_{3/2})$ products, while the $B^2\Sigma^+_{g,1/2}$ state correlates to $I^- + I^*(^2P_{1/2})$ products, lying

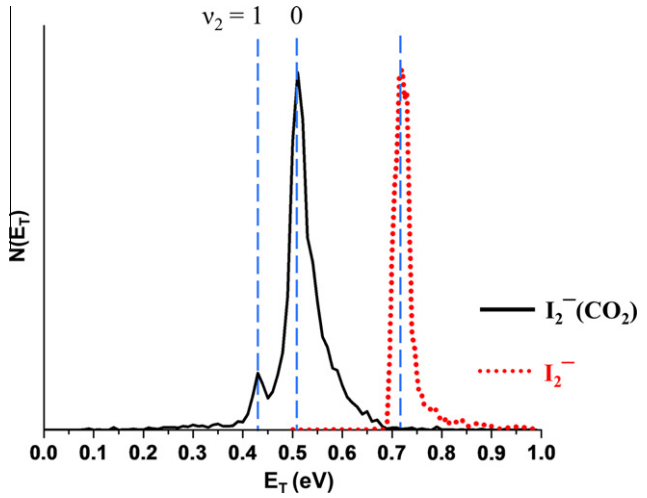

Figure 1. Translational energy distributions for the dissociation of both bare I_2^- (red, dotted line) and $I_2^-(CO_2)$ (solid, black line) following the $A'^2\Pi_{g,1/2} - X^2\Sigma^+_{u,1/2}$ transition at E_{hv} = 1.722 eV. (For interpretation of the references to colour in this figure legend, the reader is referred to the web version of this article.)

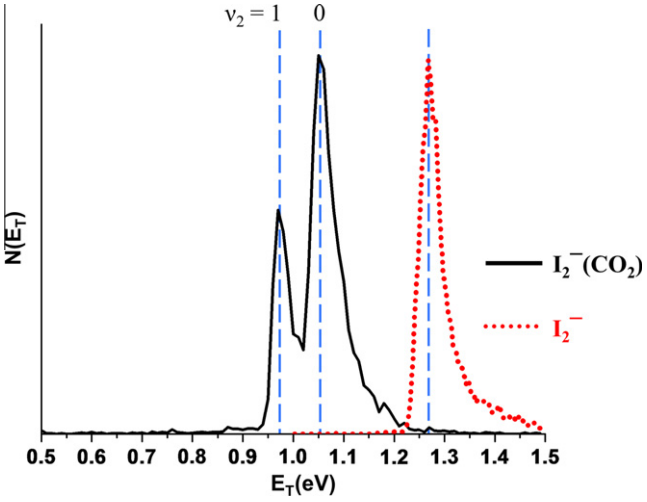

Figure 2. Translational energy distributions for the dissociation of both bare I_2^- (red, dotted line) and $I_2^-(CO_2)$ (solid, black line) following the $B^2\Sigma^+_{g,1/2} - X^2\Sigma^+_{u,1/2}$ transition at E_{hv} = 3.212 eV. (For interpretation of the references to colour in this figure legend, the reader is referred to the web version of this article.)

0.943 eV higher in energy. The two- and three-body distributions are shown as dotted and solid lines, respectively, and the dashed vertical lines indicate the peak position for each feature.

At both wavelengths, dissociation of I_2^- produces a single peak whose translational energy is determined by

$$E_T = h\nu - D_0(I_2^-) \quad (1)$$

where $D_0(I_2^-)$ is the bond dissociation energy for the relevant dissociation channel: 1.007 ± 0.005 and 1.950 ± 0.005 eV for production of $I(^2P_{3/2})$ and $I^*(^2P_{1/2})$, respectively [35]. The experimental peak positions at the two wavelengths, E_T = 0.72 eV (720 nm) and 1.26 eV (386 nm), conform to the expected values. The full-width-at-half-maximum peak widths of ~50 meV and the tail toward higher E_T reflect the internal energy of the parent I_2^- anion.

The three-body distributions for $I_2^-(CO_2)$ at both wavelengths are shifted toward lower E_T, and each distribution comprises two peaks. The dominant peaks are at 0.51 and 1.05 eV at 720 and 386 nm, respectively, so each lies ~0.21 eV below the corresponding I_2^- peak. At each wavelength, the smaller peak is shifted to

lower E_T by 80 meV with respect to the larger peak, an energy interval equal to the fundamental bending vibrational frequency in CO_2 (667 cm^{-1}). Based on the peak heights, the relative intensity of the smaller peak with the respect to the higher energy peak is approximately 16% at 720 nm and 59% at 386 nm.

3.2. Dalitz plot analysis

To gain further insight into the three-body dissociation dynamics, the momentum partitioning among the photofragments in the decay process, $f_i = p_i^2/\Sigma p_j^2$, can be represented in a Dalitz plot [33] as shown in Figure 3. Conservation of energy requires that all points representing a three-body dissociation event lie within the triangle, while conservation of momentum further requires all points to lie within the inscribed circle [8]. With unit triangle height, the radius of the inscribed circle is ⅓ with its center at (⅓, ⅓, ⅓). Points along the edge of this circle correspond to events in which the three momentum vectors are collinear, while points near the center originate from more symmetric, non-collinear fragmentation [6]. Given that the iodine atoms are indistinguishable in terms of their mass, these plots are twofold symmetric for this system about the line AB (equal iodine momenta) indicated in Figure 3. To take advantage of this symmetry, we apply a convention of plotting the iodine fragments receiving more (less) of the center of mass momentum on one axis labeled I_{fast} (I_{slow}). This convention allows the Dalitz plot to be 'folded over' with all points now confined to half of the inscribed circle [8].

Dalitz plots for dissociation from excitation to the A' and B states are shown in Figure 3a and b, respectively. These plots are similar in appearance with pronounced intensity in the region corresponding to low CO_2 momentum ($f_{CO_2} \leqslant 0.1$), indicating that most of the available momentum is taken up by the recoiling I atoms. The points are noticeably more confined near the radius of the inscribed circle in Figure 3b. These plots are discussed in more detail in Section 3.4.

3.3. Dissociation energies

In the three-body dissociation of $I_2^-(CO_2)$, the translational energy for a photodissociation event will be

$$E_T = h\nu + E_{int}\left[I_2^-(CO_2)\right] - \left[D_0(I_2^-) + D_0(I_2^- \cdot\cdot CO_2) + E_{int}(CO_2)\right], \quad (2)$$

where E_{int} refers to vibrational and rotational energy of either the parent ion or CO_2 fragment, and $D_0(I_2^- \cdot\cdot CO_2)$ is the binding energy of CO_2 to I_2^-. By comparison to Eq. (1), if the parent ion and CO_2 fragment have no internal energy, then the shift of the three-body peaks in Figures 1 and 2 compared to the two-body peaks directly yields the CO_2 binding energy.

Given that the two three-body peaks at each wavelength are separated by the CO_2 bending frequency, we assign the dominant peak to $I^- + I + CO_2(v_2 = 0)$, and the smaller peak to $I^- + I + CO_2(v_2 = 1)$, with the I atom in its $^2P_{3/2}$ or $^2P_{1/2}$ state depending on the excitation wavelength. The peak widths for the three-body features in Figures 1 and 2 are similar to those for the two-body features, indicating that the contribution from additional degrees of freedom such as CO_2 rotational energy to the three-body widths is negligible. Since the peak maxima in the two-body features give the correct I_2^- bond dissociation energy, it is reasonable to attribute the maximum of the $I^- + I + CO_2$ ($v_2 = 0$) peak to dissociation from ground state parent ions to ground state products. Hence, the difference between the maximum of this feature and that of the two-body feature is an appropriate measure of the CO_2 binding energy. Averaging this difference from data taken at both excitation energies, we obtain an average value for the binding energy of 218 ± 10 meV.

This value lies within the error of the previous cluster calorimetry measurement of 234 ± 21 meV [27]. However, the calorimetry method only measures the shift in electron affinity as a function of cluster size, providing the energy gap between the neutral and anionic cluster rather than the anion solvent binding energies. Thus, that value requires an estimate of the neutral binding energy, whereas the method described herein does not. Fitting the calorimetry data over a range of cluster sizes yielded a value of 95(±16) meV for the neutral binding energy. With the $I_2^-(CO_2)$ binding energy obtained here ($S_1^{(-)}$) and the previous measurement of the increased electron affinity of $I_2^-(CO_2)$ with respect to bare I_2^-, ΔE_a = 139 meV [24], the neutral binding energy is given by

$$S_1^{(0)} = S_1^{(-)} - \Delta E_a(1) \quad (3)$$

and found to be 80 ± 15 meV for $I_2(CO_2)$.

3.4. Three-body dissociation dynamics

From fitting and integrating the two peaks in each three-body distribution, we find that dissociation from the B state produces vibrationally excited CO_2 in approximately 34% of the three-body dissociation events as opposed to only 13% from A' state dissociation. This dependence upon excitation energy deviates from a strictly Franck–Condon (FC) model of photodissociation [36], in which the CO_2 vibrational distribution is determined by the projection of the distorted, anion-bound CO_2 geometry onto the vibrational states of linear, isolated CO_2, yielding the same vibrational

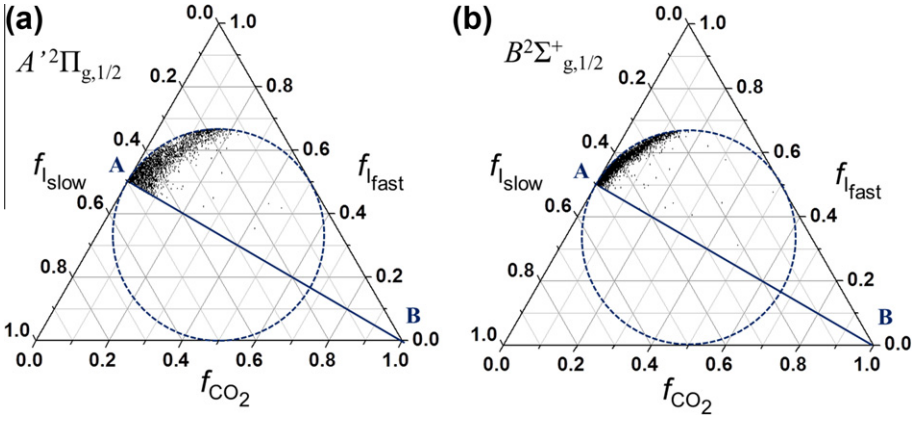

Figure 3. Dalitz plots of momentum partitioning ($f_i = p_i^2/\Sigma p_j^2$) between the fragments in three-body dissociation of $I_2^-(CO_2)$ for both transitions studied. (a) A'-state and (b) B-state. *The line AB corresponds to equal iodine momenta.

distribution for dissociation from either the A' or B state. Hence, it appears that final state interactions as the CO_2 separates from the dissociating I_2^- differ for excitation into the two I_2^- states. One can attribute these differences at least in part to the greater translational energy available to the fragments upon excitation to the B state, about 1 vs. 0.5 eV, as shown in Figures 1 and 2, but additional insights into the mechanistic origin of this effect can be gleaned from comparison with other data.

For example, the photoelectron spectrum [24] of $I_2^-(CO_2)$ shows bend excitation in the CO_2 moiety of the neutral complex comparable to that seen here in the CO_2 fragment upon excitation to the A' state. As the extent of vibrational excitation in the photoelectron spectrum is determined by the FC overlap of the bent CO_2 in $I_2^-(CO_2)$ with the linear CO_2 in neutral $I_2(CO_2)$, it appears that the simple FC picture does apply to photodissociation of $I_2^-(CO_2)$ via the A' state. In contrast, the CO_2 distribution from excitation of the B state is closer to the extent of bend excitation seen in the photoelectron spectrum of $I^-(CO_2)$, [25] where the CO_2 is more strongly bent than in $I_2^-(CO_2)$. These comparisons suggest that the CO_2 from A' state excitation is leaving from an approximately intact I_2^- moiety, while the CO_2 vibrational distribution from B state dissociation is determined more by the $I^-(CO_2)$ interaction than by the $I_2^-(CO_2)$ interaction. Such a result might indicate sequential three-body decay upon B state excitation in which the iodine bond breaks first, followed by dissociation of the $I^-(CO_2)$ fragment.

These somewhat speculative arguments can be tested by examining the Dalitz plots in Figure 3. The limiting three-body decay mechanisms inferred from these plots, which have been discussed in detail previously [4,5], can be summarized as follows. Points along the line AB represent events in which the I atoms recoil with equal and opposite momentum, with the remainder appearing as CO_2 recoil. Events at point A represent those in which zero momentum is imparted to the CO_2 fragment, which essentially acts as a spectator. As one moves away from point A along AB, there is increasing momentum taken up by the CO_2, with the three momentum vectors forming a 'T' with C_{2v} symmetry. Events along this line correspond to synchronous–concerted dissociation, in which the I–I and I_2–CO_2 bonds break simultaneously.

Points along the circumference of the inscribed circle correspond to collinear events in which all three momentum vectors are parallel; moving away from point A along the circumference corresponds to increasingly asymmetric partitioning of the momentum between the two I atoms, with the CO_2 making up the difference. This partitioning indicates an asynchronous–concerted decay mechanism, in which the second bond breaking event occurs within a vibrational period of the first. This type of decay confines both bonds to break within the original plane of the parent molecule that contains the two dissociating bonds and results in intensity along the edge of the allowed circular region. Asynchronous concerted decay is distinct from asynchronous sequential decay, in which the intermediate formed after the first bond cleavage lives on the order of a rotational period prior to dissociation. Asynchronous sequential decay leads to a constant fraction of the momentum in one fragment, as evidenced by a line segment parallel to one side of the triangle in the Dalitz plots [12,37].

In a previous study of $I_2^-(Ar)$ on our instrument [29], the dominant mechanism was synchronous–concerted dissociation with nearly zero momentum imparted to the Ar atom, i.e. events clustered around point A on the Dalitz plot. While the Dalitz plots for $I_2^-(CO_2)$ do show contributions at point A and along AB, there are considerably more dissociation events with unequal partitioning of the momenta between the iodine atoms and non-zero CO_2 momentum at both excitation energies. As with $I_2^-(Ar)$, deviations in the initial cluster geometry from strict C_{2v} symmetry owing to large amplitude vibrational motion can also result in a small number of dissociation events with unequal iodine momenta even though the dissociation remains synchronous. This mechanism should contribute to some of points lying off the line AB in the Dalitz plots for $I_2^-(CO_2)$. However, compared to $I_2^-(Ar)$, most of the signal lies well away from the AB line and there is significantly more intensity along the edge of the inscribed circle, the signature of asynchronous–concerted decay. There is no evidence for asynchronous–sequential decay.

Comparing the plots at the two wavelengths, the dissociation events from B state excitation are more confined to the diameter of the inscribed circle than those from A' state excitation. Hence, while both wavelengths are dominated by asynchronous rather than synchronous decay, the B state represents a purer case of the asynchronous–concerted mechanism, in which a short-lived $I^-(CO_2)$ fragment promptly dissociates following the initial I–I bond cleavage. This distinction may reflect the more repulsive interaction between the two I atoms in the B state than in the A' state; in the B state, the two I atoms separate rapidly, leaving the CO_2 attached to the I^- fragment, whereas in the A' state, the separation between the two bond cleavages is not as clean.

It thus appears that the distinction between the Dalitz plots at the two wavelengths is consistent with the origin of the differing CO_2 vibrational distributions that was suggested at the beginning of this section. Upon excitation of the A' state, the departing CO_2 is interacting with a dissociating I_2^- moiety, whereas B state dissociation involves a more distinct passage through a short-lived $I^-(CO_2)$ intermediate. Based on the Franck–Condon picture outlined above, these dynamics would result in more bend excitation in the CO_2 fragment from B state dissociation, consistent with the results seen in Figures 1 and 2. It would certainly be of interest to perform molecular dynamics calculations on the two excited states of the cluster to test these ideas more rigorously.

4. Conclusions

The three-body photodissociation of $I_2^-(CO_2)$ has been studied following excitation to both the $A'^2\Pi_{g,1/2}$ state at 720 nm and the $B^2\Sigma^+_{g,1/2}$ state at 386 nm of the I_2^- chromophore. The three-body translational energy distributions directly yield $D_0(I_2^- \cdot CO_2) = 218 \pm 10$ meV. These distributions are vibrationally resolved and show short progressions in the CO_2 bending mode, with more bend excitation resulting from excitation of the B state. Dalitz plots of the three-body events indicate that dissociation at both wavelengths is primarily asynchronous–concerted, although the results for the B state conform to this limit more than those for the A' state, suggesting the formation of a transient $I^-(CO_2)$ intermediate at 386 nm excitation. These differences in mechanism are proposed as the origin of the differing vibrational distributions at the two wavelengths, since the formation and dissociation of such an intermediate is likely to result in more CO_2 bend excitation than a less asynchronous mechanism.

Acknowledgments

This research was supported by the Director, Office of Basic Energy Science, Chemical Sciences Division of the US Department of Energy under Contract No. DE-AC02-05CH11231.

References

[1] Y.T. Lee, J.D. McDonald, P.R. LeBreton, D.R. Herschbach, Rev. Sci. Instrum. 40 (1969) 1402.
[2] R. Schinke, Photodissociation Dynamics, University Press Journal, Cambridge, 1993.
[3] L.J. Butler, D.M. Neumark, J. Phys. Chem. 100 (1996) 12801.
[4] C. Maul, K.-H. Gericke, Int. Rev. Phys. Chem. 16 (1997) 1.
[5] C. Maul, K.-H. Gericke, J. Phys. Chem. A 104 (2000) 2531.
[6] U. Muller, T. Eckert, M. Braun, H. Helm, Phys. Rev. Lett. 83 (1999) 2718.

[7] L.M. Dobeck, H.M. Lambert, W. Kong, P.J. Pisano, P.L. Houston, J. Phys. Chem. A 103 (1999) 10312.
[8] D. Babikov et al., J. Chem. Phys. 116 (2002) 4871.
[9] K.A. Hanold, A.K. Luong, R.E. Continetti, J. Chem. Phys. 109 (1998) 9215.
[10] J.D. Savee, V.A. Mozhayskiy, J.E. Mann, A.I. Krylov, R.E. Continetti, Science 321 (2008) 826.
[11] P. Jukes, A. Buxey, A.B. Jones, A.J. Stace, J. Chem. Phys. 109 (1998) 5803.
[12] A. Matsuda, M. Fushitani, R.A. Thomas, V. Zhaunerchyk, A. Hishikawa, J. Phys. Chem. A 113 (2009) 2254.
[13] B.J. Greenblatt, M.T. Zanni, D.M. Neumark, Chem. Phys. Lett. 258 (1996) 523.
[14] M.T. Zanni, V.S. Batista, B.J. Greenblatt, W.H. Miller, D.M. Neumark, J. Chem. Phys. 110 (1999) 3748.
[15] D. Ray, N.E. Levinger, J.M. Papanikolas, W.C. Lineberger, J. Chem. Phys. 91 (1989) 6533.
[16] J.M. Papanikolas, V. Vorsa, M.E. Nadal, P.J. Campagnola, J.R. Gord, W.C. Lineberger, J. Chem. Phys. 97 (1992) 7002.
[17] B.J. Greenblatt, M.T. Zanni, D.M. Neumark, J. Chem. Phys. 111 (1999) 10566.
[18] A.V. Davis, R. Wester, A.E. Bragg, D.M. Neumark, J. Chem. Phys. 119 (2003) 2020.
[19] R. Parson, J. Faeder, N. Delaney, J. Phys. Chem. A 104 (2000) 9653.
[20] D.A.V. Kliner, J.C. Alfano, P.F. Barbara, J. Chem. Phys. 98 (1993) 5375.
[21] P.K. Walhout, J.C. Alfano, K.A.M. Thakur, P.F. Barbara, J. Phys. Chem. 99 (1995) 7568.
[22] L. Sheps, E.M. Miller, S. Horvath, M.A. Thompson, R. Parson, A.B. McCoy, W.C. Lineberger, Science 328 (2010) 220.
[23] L. Sheps, E.M. Miller, S. Horvath, M.A. Thompson, R. Parson, A.B. McCoy, W.C. Lineberger, J. Chem. Phys. 134 (2011) 184311.
[24] H. Gomez, T.R. Taylor, D.M. Neumark, J. Chem. Phys. 116 (2002) 6111.
[25] D.W. Arnold, S.E. Bradforth, E.H. Kim, D.M. Neumark, J. Chem. Phys. 102 (1995) 3510.
[26] A.K. Pathak, T. Mukherjee, D.K. Maity, J. Phys. Chem. A 112 (2008) 12037.
[27] R. Wester, A.V. Davis, A.E. Bragg, D.M. Neumark, Phys. Rev. A 65 (2002) 051201.
[28] R.E. Continetti, D.R. Cyr, R.B. Metz, D.M. Neumark, Chem. Phys. Lett. 182 (1991) 406.
[29] A.A. Hoops, J.R. Gascooke, A.E. Faulhaber, K.E. Kautzman, D.M. Neumark, Chem. Phys. Lett. 374 (2003) 235.
[30] J.M.B. Bakker, J. Phys. E 6 (1973) 785.
[31] J.M.B. Bakker, J. Phys. E 7 (1974) 364.
[32] Z. Amitay, D. Zajfman, Rev. Sci. Instrum. 68 (1997) 1387.
[33] R.H. Dalitz, Philos. Mag. 44 (1953) 1068.
[34] E.C.M. Chen, W.E. Wentworth, J. Phys. Chem. 89 (1985) 4099.
[35] M.T. Zanni, T.R. Taylor, B.J. Greenblatt, B. Soep, D.M. Neumark, J. Chem. Phys. 107 (1997) 7613.
[36] Y.B. Band, K.F. Freed, J. Chem. Phys. 67 (1977) 1462.
[37] P.E. Crider, A.W. Harrison, D.M. Neumark, J. Chem. Phys. 134 (2011) 134306.